Confluent Vessel Trees with Accurate Bifurcations Supplementary Materials

Zhongwen Zhang[1] Dmitrii Marin[1,2] Maria Drangova[3] Yuri Boykov[1,2]

[1]University of Waterloo, Canada [2]Vector Research Institute, Canada [3]Robarts Research, Canada

PROPERTY 1. *The angle between* $\breve{c}^1_{pq}$ *and* $\bar{l}_q$ *is equal to the angle between* $\breve{c}^1_{qp}$ *and* $\bar{l}_p$*. That is,*

$$\angle(\breve{c}^1_{pq}, \breve{c}^0_{qp}) \equiv \angle(\breve{c}^1_{qp}, \breve{c}^0_{pq}). \tag{1}$$

Proof. First, we only consider the circle going through p, q and tangential to some vector $\bar{\tau}_p$ as shown in Fig. 1. Moving the tangent vector $\bar{\tau}_p$ in its direction along the circle yields another tangent vector $\bar{\tau}_q$ at q. We also translate $\bar{\tau}_p$ to q. By construction, ΔOpq is equilateral. Thus, $\angle Opq = \angle Oqp$. Since $\bar{\tau}_p$ and $\bar{\tau}_q$ are tangential to the circle, we have $\alpha + \angle Opq = \beta + \angle Oqp = \frac{\pi}{2}$, which obviously gives $\alpha = \beta$. WLOG, we assume vectors $\bar{\tau}_p$, $\bar{\tau}_q$ and $\bar{e}$ are all unit vectors. As $\alpha = \beta$, we have:

$$\bar{\tau}_q = 2[(\bar{\tau}_p \cdot \bar{e})\bar{e} - \bar{\tau}_p] + \bar{\tau}_p \tag{2}$$

Now, we consider the two circles going through both p and q while one is tangential to $\bar{l}_p$ and the other is tangential to the $\bar{l}_q$ as shown in Fig. 2. Note that these two circles are not necessarily co-planar. Using (2), we can obtain

$$\breve{c}^1_{pq} = 2[(\breve{c}^0_{pq} \cdot \vec{e}_1)\vec{e}_1 - \breve{c}^0_{pq}] + \breve{c}^0_{pq} \tag{3}$$

$$\breve{c}^1_{qp} = 2[(\breve{c}^0_{qp} \cdot \vec{e}_1)\vec{e}_1 - \breve{c}^0_{qp}] + \breve{c}^0_{qp} \tag{4}$$

To prove (1), it is sufficient to prove equality of the two dot products which can be simplified using (3) and (4):

$$\breve{c}^1_{pq} \cdot \breve{c}^0_{qp} = 2(\breve{c}^0_{pq} \cdot \vec{e}_1)(\breve{c}^0_{qp} \cdot \vec{e}_1) - \breve{c}^0_{pq} \cdot \breve{c}^0_{qp} \tag{5}$$

$$\breve{c}^1_{qp} \cdot \breve{c}^0_{pq} = 2(\breve{c}^0_{qp} \cdot \vec{e}_1)(\breve{c}^0_{pq} \cdot \vec{e}_1) - \breve{c}^0_{qp} \cdot \breve{c}^0_{pq} \tag{6}$$

It is obvious that the RHS of (5) and (6) are equal. Therefore, these two angles are equal. □

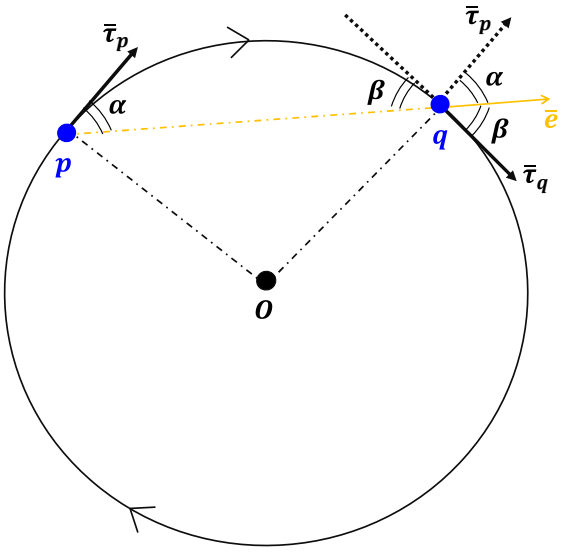

Figure 1: Illustration for (2). O is the center of the circle. $\bar{e}$ is a unit vector along pq.

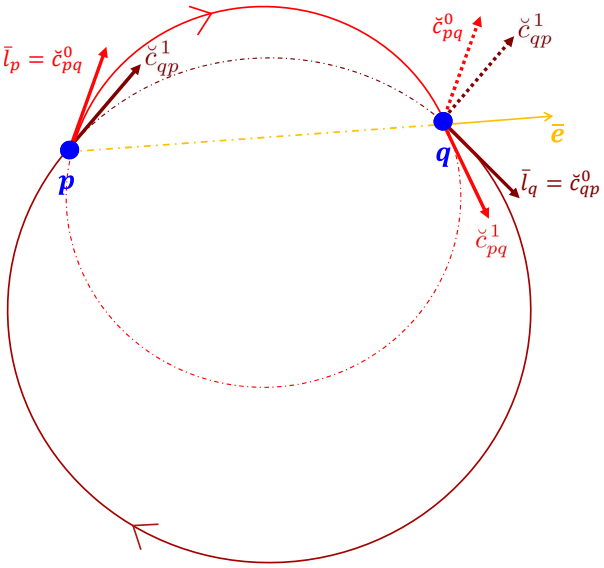

Figure 2: Two circles given by p,q, $\breve{c}^0_{pq}$ and $\breve{c}^0_{qp}$. Vectors in red are co-planar with the red circle while those in maroon are co-planar with the maroon circle.

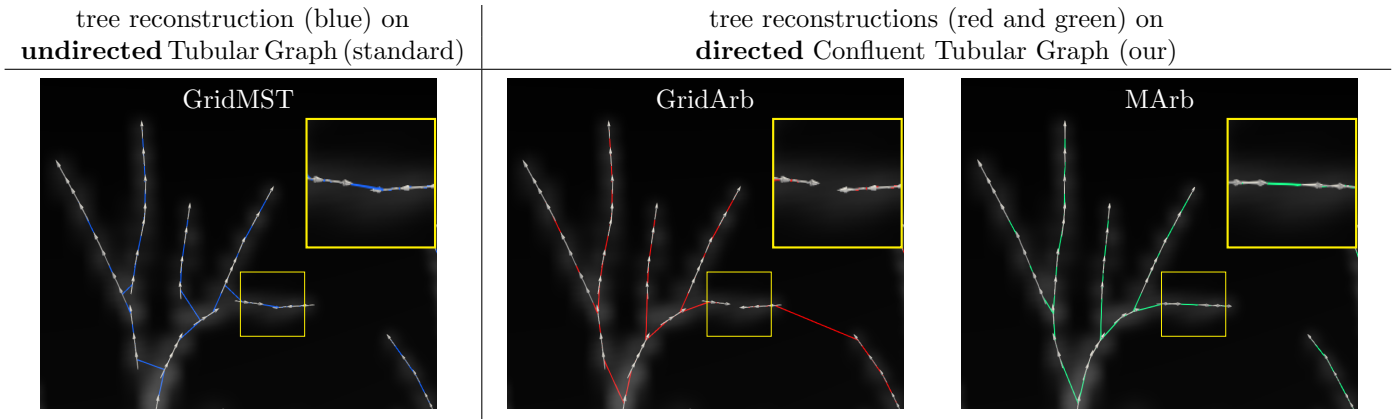

(a) Flow pattern estimate (white) [3] + MST on geodesic tubular graph

(b) Flow pattern estimate (white) [3] + min. arb. on confluent tubular graph

(c) *Improved* flow estimate (white) + min. arb. on confluent tubular graph

Figure 3: Typical tree reconstruction examples for standard (a) and our *confluent* (b,c) tubular graphs. (a) White vectors represent CRF-based flow pattern estimates [3] using 26-grid regularization neighborhood $\mathcal{N}$. In case of thin sub-voxel vessels, such $\mathcal{N}$ has gaps creating inconsistent flow pattern for isolated small branches (yellow box) lacking bifurcations used by divergence prior to disambiguate orientations. (a) Undirected geodesic tubular graph with large KNN easily bridges such gaps ignoring (inconsistent) flow directions and produces topologically valid vessel MST (blue), even though bifurcations are not accurate. (b) Directed confluent tubular graph is sensitive to flow pattern errors. Minimum arborescence on this graph produces accurate bifurcations, but flow orientation errors (yellow box) lead to wrong topology. (c) CRF-based flow pattern estimator [3] with modified anisotropic KNN system $\mathcal{N}$ addresses the gaps at thin vessels. This improves flow orientations (white vectors in yellow box) and resolves confluent tubular graph artifacts producing trees with accurate both topology and bifurcations.

CRF Regularization Neighborhood

Our tree extraction method is based on a directed *confluent tubular graph* construction $G = \langle V, A \rangle$ presented in Sec. 3 of the paper. We proposed an approach that builds confluent flow-extrapolating arcs $\breve{c}_{pq}$ for our graph from estimated *oriented* flow vectors $\{\bar{l}_p \,|\, p \in V\}$. Specific flow orientations can be computed from Frangi filter outputs using standard MRF/CRF regularization methods [3] enforcing divergence (or convergence) of the flow pattern. However, as mentioned in Sec. 3.3 and Sec. 4, we modified [3] by anisotropically enlarging the regularization neighborhood to improve the estimates of flow orientations, which are important for our directed arc construction. The 26-grid neighborhood regularization used in [3] generates too many CRF connectivity gaps near the vessel tree periphery where the signal gets weaker. Such gaps result in flow orientation errors, see white vectors in the zoom-ins in Fig. 3(a,b). While tree reconstruction on standard undirected geodesic tubular graphs, see Fig. 3(a), are oblivious to such errors, our directed *confluent tubular graph* construction is sensitive to wrong orientations, see Fig. 3(b). To address CRF gaps in the flow orientation estimator [3], we modified their 26-grid regularization neighborhood into *anisotropic KNN* based on Frangi's vessel tangents [1]. This significantly reduces orientation errors in $\{\bar{l}_p \,|\, p \in V\}$ and resolves confluent tubular graph artifacts, see Fig. 3(c). We detail anisotropic KNN below.

CRF connectivity quality: Besides the size of the neighborhood K, anisotropic KNN system has another important hyper-parameter, aspect ratio ar. To select better parameters K and ar, we can evaluate CRF connectivity system $\mathcal{N}$ using ROC curves for synthetic vasculature volumes with ground truth. We consider an edge in $\mathcal{N}$ as *correct* iff the projections of its ends onto the ground truth tree have parent/descendant relationship. The *recall* is the portion of the ground truth tree covered by the correct edges. The *fall-out* is the ratio of incorrect edges to the total edge count.

As shown in Fig. 4, simply increasing the size of neighborhood closes many gaps but, in the meantime, introduces a lot of spurious connections between different vessel branches. Thus, we propose to use anisotropic neighborhoods. Specifically, the regularization neighborhood is redefined as k anisotropic nearest neighbors instead of regular grid connectivity. This similar to the KNN except Mahalanobis distance is used. This modification addresses the issue giving

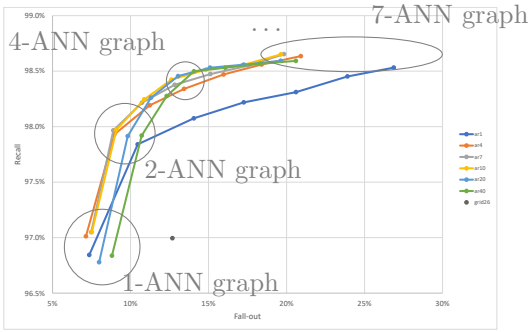

Figure 4: (Quasi) ROC curves evaluating accuracy of the neighborhoods N used for flow pattern estimation, as in [3]. We compare anisotropic KNNs and standard 26-grid connectivity (see gray dot). Evaluation is done based on synthetic data with ground truth where correct connectivity is available. "ar" stands for the aspect ratio and the number denotes the square of the aspect ratio. "grid26" represent the regular 26 neighbors on grid. We select "ar10" with 4 anisotropic nearest neighbourhood (ANN) connectivity system.

the state-of-the-art result, see Fig.3(c). To implement such anisotropic neighborhood system, we first built an isotropic KNN with some large K, eg. K=500. Then, for each node and its neighbors, we transformed the Euclidean distance into Mahalanobis distance based on the tangent direction on the node. After this, we selected K (eg. K=4) nearest neighbors for each node again based on the Mahalnobis distance. Note that such anisotropic neighborhood is symmetric since we consider a pair of nodes as neighbor as long as one is connected to the other.

Angular Error Measure

The *average* angular error introduced in [3] uses only correctly detected points to compute the bifurcation angular errors. Using such matching to compare different methods is unfair as for a particular detection threshold these methods correctly detect different sets of bifurcations. So, we match *all* ground truth bifurcations to closet branching points on the detected tree regardless of their proximity. For certain thresholds, this causes many incorrectly matched bifurcation and large errors. Despite that such statistic is influenced significantly by random matches, it is meaningful for comparing different reconstruction methods.

Synthetic Data with Ground Truth

Zhang *et al.* [3] generated and published a dataset with ground truth using [2]. We found that the diversity of bifurcation angles is limited. The mean angle is 68° and *std* is 17°. To increase the angle variance, we introduce a simple modification of vessel tree generation. When a new bifurcation is created from a point and existing line segment, we move the bifurcation towards one of the segment's ends chosen at random decreasing the distance by half. The new mean is 68° and *std* is 29°. We generate 15 volumes 100×100×100 with intensities between 0 and 512. The voxel size is 0.046 mm. We add Gaussian noise with *std* 10 and 15.

References

[1] Alejandro F Frangi, Wiro J Niessen, Koen L Vincken, and Max A Viergever. Multiscale vessel enhancement filtering. In *MICCAI'98*, pages 130–137. Springer, 1998. 2

[2] Ghassan Hamarneh and Preet Jassi. Vascusynth: simulating vascular trees for generating volumetric image data with ground-truth segmentation and tree analysis. *Computerized medical imaging and graphics*, 34(8):605–616, 2010. 3

[3] Zhongwen Zhang, Dmitrii Marin, Egor Chesakov, Marc Moreno Maza, Maria Drangova, and Yuri Boykov. Divergence prior and vessel-tree reconstruction. In *IEEE conference on Computer Vision and Pattern Recognition (CVPR)*, Long Beach, California, June 2019. 2, 3